Research Article Vol. 2, No. 7 / July 2015 / Optica 635

Optomechanical creation of magnetic fields for photons on a lattice

M. Schmidt,[1] S. Kessler,[1] V. Peano,[1] O. Painter,[2] and F. Marquardt[1,3,*]

[1]University of Erlangen-Nürnberg, Staudtstr. 7, Institute for Theoretical Physics, D-91058 Erlangen, Germany
[2]Institute for Quantum Information and Matter and Thomas J. Watson, Sr., Laboratory of Applied Physics, California Institute of Technology, Pasadena, California 91125, USA
[3]Max Planck Institute for the Science of Light, Günther-Scharowsky-Straße 1/Bau 24, D-91058 Erlangen, Germany
*Corresponding author: Florian.Marquardt@fau.de

Received 15 April 2015; revised 8 June 2015; accepted 8 June 2015 (Doc. ID 238089); published 10 July 2015

Recently, there has been growing interest in the creation of artificial magnetic fields for uncharged particles, such as cold atoms or photons. These efforts are partly motivated by the resulting desirable features, such as transport along edge states that is robust against backscattering. We analyze how the optomechanical interaction between photons and mechanical vibrations can be used to create artificial magnetic fields for photons on a lattice. The ingredients required are an optomechanical crystal, i.e., a free-standing photonic crystal with localized vibrational and optical modes, and two laser beams with the right pattern of phases. One of the two schemes analyzed here is based on optomechanical modulation of the links between optical modes, while the other is a lattice extension of optomechanical wavelength-conversion setups. We analyze both schemes theoretically and present numerical simulations of the resulting optical spectrum, photon transport in the presence of an artificial Lorentz force, edge states, and the photonic Aharonov–Bohm effect. We discuss the requirements for experimental realizations. Finally, we analyze the completely general situation of an optomechanical system subject to an arbitrary optical phase pattern and conclude that it is best described in terms of gauge fields acting in synthetic dimensions. In contrast to existing nonoptomechanical approaches, the schemes analyzed here are very versatile, since they can be controlled fully optically, allowing for time-dependent *in situ* tunability without the need for individual electrical addressing of localized optical modes.

OCIS codes: (230.5298) Photonic crystals; (230.4555) Coupled resonators; (230.4685) Optical microelectromechanical devices.

http://dx.doi.org/10.1364/OPTICA.2.000635

1. INTRODUCTION

Light interacting with nano-mechanical motion via the radiation pressure force is studied in the field of optomechanics. The field has seen rapid progress in the last few years (see the recent review [1]). So far, most experimental achievements have been realized in setups comprising one optical mode coupled to one vibrational mode. Obviously, one of the next frontiers will be the combination of many such optomechanical cells into an optomechanical array, enabling the optical *in situ* investigation of (quantum) many-body dynamics of interacting photons and phonons. Many experimental platforms can be scaled up to arrays. However, optomechanical crystals seem to be the best-suited candidates at the present stage. Optomechanical crystals are formed by the periodic spatial patterning of regular dielectric and elastic materials, resulting in an enhanced coupling between optical and acoustic waves via moving boundary or electrostriction radiation pressure effects. Two-dimensional (2D) optomechanical crystals with both photonic and phononic bandgaps [2] can be fabricated by standard microfabrication techniques through the lithographic patterning, plasma etching, and release of a thin-film material [3]. These 2D crystals for light and sound can be used to create a circuit architecture for the routing and localization of photons and phonons [3–7].

Optomechanical arrays promise to be a versatile platform for exploring optomechanical many-body physics. Several aspects have already been investigated theoretically, e.g., synchronization [8–10], long-range interactions [11,12], reservoir engineering [13], entanglement [14,15], correlated quantum many-body states [10], slow light [16], transport in a one-dimensional (1D) chain [17], and graphene-like Dirac physics [18].

One of the central aims in photonics is to build waveguides that are robust against disorder and do not display backscattering. Recently there have been several proposals [19–23] to engineer nonreciprocal transport for photons. On the lattice, this corresponds to an artificial magnetic field, which would (among other effects) enable chiral edge states that display the desired robustness against disorder. First experiments have shown such edge states [24–26]. These developments in photonics are related to a growing effort across various fields to produce synthetic gauge fields for neutral particles [27–30].

In this paper we will propose two schemes to generate arbitrary artificial magnetic fields for photons on a lattice. These schemes break time-reversal symmetry by incorporating amplitude-modulated laser fields with different modulation phases at different sites. In contrast to any previous proposals or experiments for photonic magnetic fields on a lattice, these would be controlled all-optically, and, crucially, they would be tunable *in situ* by changing the properties of a laser field (frequency, intensity, and phase pattern). They require no more than a patterned dielectric slab illuminated by two laser beams with suitably engineered optical phase fields. The crucial ingredient is the optomechanical interaction.

2. OPTOMECHANICAL SCHEMES FOR PHOTON MAGNETIC FIELDS

On the classical level, a charged particle subject to a magnetic field experiences a Lorentz force. In the quantum regime, the appearance of Landau levels leads to the integer and fractional quantum Hall effects, where topologically protected chiral edge states are responsible for a quantized Hall conductance. On a closed orbit, a particle with charge q will pick up a phase that is given by the magnetic flux Φ through the circumscribed area, where $\Phi = (q/\hbar)\int \mathbf{B}\cdot \mathrm{d}\mathbf{S}$ in units of the flux quantum, with $\mathbf{B}$ denoting the magnetic field. On a lattice, a charged particle hopping from site i to j acquires a Peierls phase $\phi_{ij} = (q/\hbar)\int_{\mathbf{r}_i}^{\mathbf{r}_j} \mathbf{A}\mathrm{d}\mathbf{r}$ determined by the vector potential $\mathbf{A}$. Conversely, if we can engineer a Hamiltonian for neutral particles containing arbitrary Peierls phases,

$$\hat{H}_{\mathrm{hop}} = \hbar J \sum_{\langle ij\rangle} e^{i\phi_{ij}} \hat{a}_j^\dagger \hat{a}_i + \mathrm{h.c.}, \quad \textbf{(1)}$$

we are able to produce a synthetic magnetic field. Here $\hat{a}_i$ is the (bosonic) annihilation operator on lattice site i. We note in passing that different phase configurations can lead to identical flux patterns, reflecting the gauge invariance of Maxwell's equations under the transformation $\mathbf{A} \to \mathbf{A} + \nabla\xi(\mathbf{r})$ for any scalar function ξ.

A. Optomechanical Interaction as a Tool for Generating Synthetic Magnetic Fields

Every defect in an optomechanical crystal [3–7] supports a localized vibrational mode (annihilation operator $\hat{b}$, eigenfrequency Ω_0) and an optical mode ($\hat{a}$, frequency ω_{cav}) that interact via radiation pressure, giving rise to the standard optomechanical interaction [1],

$$\hat{H}_{\mathrm{int}} = -\hbar g_0 \hat{a}^\dagger \hat{a}(\hat{b}^\dagger + \hat{b}). \quad \textbf{(2)}$$

This can be utilized in two basic ways to introduce phases for the hopping of photons. First, one can drive the optical mode by a control laser (frequency ω_L) close to the red sideband, $\omega_L \sim \omega_{\mathrm{cav}} - \Omega_0$. Following the standard procedure of linearization and rotating wave approximation (RWA) [1] one recovers a swap Hamiltonian, $g\hat{a}^\dagger\hat{b} + \mathrm{h.c.}$, in which the phase ϕ of the coupling $g \in \mathbb{C}$ is set by the control laser phase. We will show below how this can be used to create a photonic gauge field. There is, however, also a second route, namely, driving the vibrational mode into a large amplitude coherent state, $\langle\hat{b}(t)\rangle = |\beta|e^{-i(\Omega t+\phi)}$, using the radiation pressure force. These oscillations then weakly modulate the optical eigenfrequency, $\omega_{\mathrm{cav}}(t) = \omega_{\mathrm{cav},0} + 2g_0|\beta|\cos(\Omega t + \phi)$, with the phase ϕ set by the oscillations. Again, in a suitable setting this will lead to an artificial magnetic field for the photons. With both of our proposed schemes it is possible to generate arbitrary gauge field configurations. This is achievable because by engineering the spatial structure of the laser phase pattern one can obtain an arbitrary configuration of photon hopping phases on the lattice, leading to an arbitrary magnetic flux distribution. We now describe both methods in turn.

B. Modulated-Link Scheme

Recently Fang *et al.* [22,31] proposed to create a photonic gauge field by electro-optically modulating the photon hopping rate $J_{ij} = J\cos(\Omega t + \phi_{ij})$ between neighboring cavities. This would require locally wired electrodes for each link of the lattice. Here we propose a potentially more powerful all-optical implementation of that idea. We employ optomechanically driven photon transitions, as first discussed in [32], but extended to a scheme with modulated interface modes, depicted in Fig. 1(a). We now discuss the leftmost three optical modes in the first row, $\hat{a}_A$, $\hat{a}_I$, and $\hat{a}_B$ (from left to right), exemplary of the full grid. Their coherent dynamics are governed by the Hamiltonian

$$\hat{H}/\hbar = \sum_{i=A,B} \omega_i \hat{a}_i^\dagger \hat{a}_i + \omega_I(t)\hat{a}_I^\dagger\hat{a}_I - J(\hat{a}_I^\dagger\hat{a}_A + \hat{a}_B^\dagger\hat{a}_I + \mathrm{h.c.}). \quad \textbf{(3)}$$

The terms describe, in this order, the first (A) and third (B) optical modes, the temporally modulated interface mode (I), and its tight-binding coupling to the neighboring A and B modes with photon tunneling rate J. As discussed further below, the eigenfrequency $\bar{\omega}_I$ of the interface mode should be well separated from

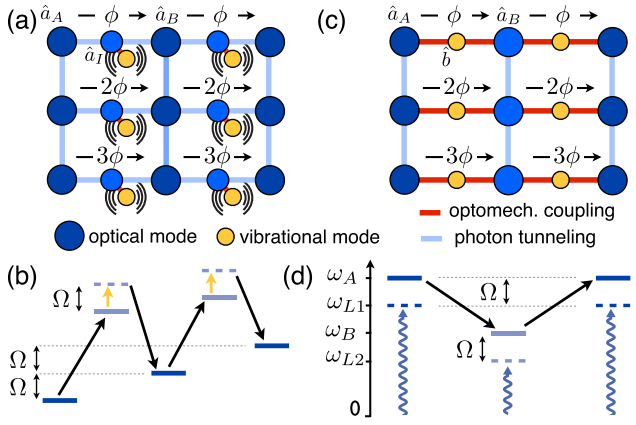

Fig. 1. Proposed schemes to create a photonic gauge field in optomechanical arrays by engineering photon hopping phases. (a) Modulated-link scheme. (b) Corresponding optical spectrum of a row with relevant sidebands (dashed). Driven vibrational modes (yellow) optomechanically modulate the frequency of optical link modes. Tunneling photons are thus upconverted to the first sideband and pick up the phase of the modulation. Arrows in (b) indicate the resonant photon transmission process in a row. (c) Wavelength-conversion scheme and (d) corresponding optical spectrum: neighboring modes in a row couple to a vibrational mode (yellow) optomechanically (red lines, denoting the linearized optomechanical interaction). Two lasers, driving the optical modes close to the red sidebands [wiggly arrows in (d)], give rise to resonant photon–phonon–photon conversion with the phase set by the lasers. Different rows are connected via simple photon hopping (blue lines), without a phase, in both schemes (a),(c). The indicated phase configuration corresponds to a constant magnetic field.

the eigenfrequencies of the adjacent A and B modes, for the transition A–I–B to be virtual. The interface mode is optomechanically coupled to a mechanical mode, which itself is driven into a large amplitude coherent state. As mentioned above, this gives rise to a weak modulation of its optical eigenfrequency, $\omega_I(t) = \bar{\omega}_I + 2g_0|\beta|\cos(\Omega t + \phi)$, with the phase ϕ set by the driving. The required mechanical driving is easily generated by two-tone laser excitation at a frequency difference Ω. The beating between the laser beams gives rise to a sinusoidal radiation pressure force, which drives the mechanical mode. If $\omega_B = \omega_A + \Omega$, then a photon hopping from site A to B picks up the phase ϕ of the modulation: starting from $\hat{a}_A$, it tunnels into $\hat{a}_I$, where it is inelastically upscattered into the first sideband by the modulation and subsequently tunnels into $\hat{a}_B$ resonantly, as shown by the spectrum in Fig. 1(b). We can derive an effective Hamiltonian, $\hbar J_{\mathrm{eff}} e^{i\phi}\hat{a}_B^\dagger \hat{a}_A + \mathrm{h.c.}$, for this process by integrating out the interface mode I using Floquet perturbative methods to third order (see Supplement 1). For the effective hopping rate we find $J_{\mathrm{eff}} = g_0|\beta|J^2/[(\omega_A - \omega_I)(\omega_B - \omega_I)]$, to leading order in J and $|\beta|$. Concatenating such three-mode blocks, we create a linear chain [the first row in Fig. 1(a)], with its optical spectrum schematically depicted in Fig. 1(b). Every time a photon hops to the right, it is upconverted and picks up the phase of the drive. To obtain a 2D grid, we stack identical chains and connect neighboring rows by direct photon hopping (whose rate must be chosen to equal J_{eff}, to obtain isotropic hopping), as depicted in Fig. 1(b). The phase configuration in Fig. 1(a) corresponds to a constant magnetic field. Note that in contrast to the general Hamiltonian (1), this scheme does not allow for phases when hopping between rows, yet it is still possible to achieve an arbitrary flux through every plaquette. Hence, arbitrary spatial distributions of magnetic flux can be generated, provided that one can control the driving laser phase at every interface mode. With the help of wave front engineering, this can be achieved with no more than two lasers: a homogeneous 'carrier' beam $E_1 = E_{10}e^{-i\omega_L t}$ and a 'modulation' beam $E_2 = E_{20}e^{-i(\omega_L+\Omega)t - i\phi(x,y)}$, with an imprinted phase pattern $\phi(x,y)$. Interference yields the desired temporally modulated intensity $|E_{10}|^2 + |E_{20}|^2 + 2\,\mathrm{Re}[E_{10}^* E_{20} e^{-i(\omega_L t + \phi(x,y))}]$, exerting a radiation force with a site-dependent phase. Care has to be taken to avoid exciting other vibrational modes (those not at the interface mode), by engineering them to have different mechanical frequencies. To this end, the driving frequency Ω would usually be chosen close to the mechanical eigenfrequency Ω_0, so the mechanical amplitude is enhanced by the mechanical quality factor and is thus much larger than any spurious amplitude in other (off-resonant) modes. By engineering the intensity pattern $|E_{20}(x,y)|$ as well, one could suppress any such unwanted effects even further.

Note that interface sites are not required for the creation of a spatially constant magnetic field. Instead, it is sufficient to modulate the sites themselves, as proposed in [33] for the case of optical lattices (see also Refs. [34,35]). The modulation can be accomplished by driving a suitable vibrational mode on the site in the same way as discussed for the links before. In this situation, a photon is upconverted at site A by the modulation, picks up the corresponding phase ϕ_A, and subsequently tunnels resonantly to the neighboring site B (which has to be chosen resonant with the sideband, i.e., $\omega_B = \omega_A + \Omega$). In addition, there is another equally important contribution to the effective tunneling rate: the photon can virtually tunnel into the neighboring site B, where it is resonantly upconverted, acquiring the phase ϕ_B. For a constant magnetic field, the phases in a row are equal, i.e., $\phi_A = \phi_B$, and both processes add up equally to the effective hopping rate. However, if one wants to go to arbitrary flux patterns, the phases would have to become unequal, and, as a result, the magnitude of the hopping amplitude, $|J_{\mathrm{eff}}| \sim |\exp(i\phi_A) + \exp(i\phi_B)|$, would start to depend on the values of those phases. This would be an undesirable feature, since it couples the hopping amplitudes to the flux distribution. Therefore, the links remain beneficial in a more general situation with arbitrary spatial flux configurations, allowing for more flexibility. In addition, if one wants to include photon–phonon coupling on the sites (as discussed in Section 4), then the links permit us to spatially separate the externally driven vibrational mode that generates the artificial field from the dynamical vibrational modes on the sites themselves.

C. Wavelength-Conversion Scheme

There is another, alternative way of engineering an optical Peierls phase, and it is related to optomechanical wavelength conversion [36,37]. In wavelength-conversion setups, low-frequency photons in one mode are upconverted to a higher frequency in another mode by exploiting the modes' mutual optomechanical coupling to a vibrational mode. We propose to scale up this idea into a grid as depicted in Fig. 1(c). The leftmost three modes in the first row depict (in this order) an optical mode (annihilation operator $\hat{a}_A$, frequency ω_A), a mechanical mode ($\hat{b}$, Ω_0), and another optical mode ($\hat{a}_B$, $\omega_B \neq \omega_A$). The mechanical mode couples optomechanically to both optical modes. A and B are driven by a laser with frequency ω_{L1} and ω_{L2}, respectively: for mode A, we require $\omega_A - \omega_{L1} = \Omega_0 + \delta \equiv \Omega$, where ω_{L1} denotes the driving laser's frequency and $\delta \ll \Omega_0$ is the detuning from the red sideband. For mode B, a similar relation $\omega_B - \omega_{L2} = \Omega$ holds, as depicted in the spectrum in Fig. 1(d). After application of the standard linearization and RWA procedure [1], the dynamics in a frame rotating with the drive are governed by the Hamiltonian

$$\hat{H}/\hbar = \Omega \sum_{i=A,B} \hat{a}_i^\dagger \hat{a}_i + \Omega_0 \hat{b}^\dagger \hat{b} - (g_A^* \hat{a}_A \hat{b}^\dagger + g_B \hat{a}_B^\dagger \hat{b} + \mathrm{h.c.}). \quad (4)$$

Elimination of the mechanical mode leads to an effective Hamiltonian $\hbar J_{\mathrm{eff}} e^{i\phi}\hat{a}_B^\dagger \hat{a}_A + \mathrm{h.c.}$ to leading order in $|g_{A,B}|/\delta$, with effective hopping rate $J_{\mathrm{eff}} = |g_A||g_B|/\delta$ and hopping phase $\phi = \phi_B - \phi_A$. Here, ϕ_A and ϕ_B are the phases of the linearized optomechanical interaction, of the form $g_A = |g_A|e^{i\phi_A}$, which are set by the phase of the laser drive at the corresponding site. Connecting alternating A and B sites by mechanical link modes yields a row whose spectrum is depicted in Fig. 1(d). As in the previous scheme, we can simply connect rows by photonic hopping without phases (at a rate J_{eff}) to yield a 2D grid. Phase front engineering of the two driving lasers is sufficient to realize arbitrary magnetic fields for photons in the grid. We note that the scheme also works for driving far away from the red sideband (yielding enhanced values of Ω and thereby J_{eff}; see below), though that requires stronger driving.

D. Comparison with Other Schemes

In general, a variety of schemes exist for nonreciprocal photon transport on a lattice, both as proposals and (partially) as proof-of-principle implementations. In comparison to those, the optomechanical schemes provide all-optical control as a crucial novel advantage. The resulting *in situ* tunability sets them

apart from existing schemes based on geometry (e.g., those based on suitably coupled ring resonators [20]). At the same time, everything is controlled by the laser phase pattern, avoiding the challenging fabrication overhead required in other tunable schemes (e.g., those with local electrodes for modulation of photon tunneling between localized optical modes [22]).

Another optomechanical scheme for nonreciprocal photon transport that could potentially be extended to a lattice is based on optical microring resonators [23], but the connection of such rather large rings via waveguides would presumably result in a less compact structure than what can be done with the photonic-crystal-based approaches analyzed here.

E. Limitations

We now discuss the limitations imposed on the achievable effective hopping $J_{\rm eff}$. The important end result will be that $J_{\rm eff}$ is limited to about the mechanical frequency Ω_0, even though perturbation theory would seem to imply a far smaller limit (for possible technical limitations connected to the driving strength, see Supplement 1).

We denote as $\epsilon \ll 1$ the order of the three small parameters $J/|\omega_A - \omega_I|$, $J/|\omega_B - \omega_I|$, and $g_0|\beta|/\Omega$ in the modulated-link scheme [Figs. 1(a) and 1(b)]. Then the effective coupling strength in the perturbative regime reads $J_{\rm eff} = \mathcal{O}(\epsilon^3)\Omega$. Even though the modulation frequency Ω need not equal the eigenfrequency Ω_0, they should usually be close to yield a significant mechanical response and avoid other resonances. For the wavelength-conversion scheme, where $|g_{A,B}|/\delta = \mathcal{O}(\epsilon)$, we recover $J_{\rm eff} = \mathcal{O}(\epsilon^2)\delta = \mathcal{O}(\epsilon^3)\Omega_0$, since RWA requires δ/Ω_0 to be small as well. In any experimental realization, photons will decay at the rate κ. Thus they travel $\sim J_{\rm eff}/\kappa \sim (\Omega_0/\kappa)\mathcal{O}(\epsilon^3)$ sites. In order for the photons to feel the magnetic field (or to find nontrivial transport at all), this number should be larger than 1. That precludes being in the deep perturbative limit $\epsilon \ll 1$, even for a fairly well sideband-resolved system (where typically $\kappa \sim 0.1\Omega_0$). Similar considerations apply for other proposed (nonoptomechanical) schemes based on modulation [22].

3. NUMERICAL SIMULATIONS

A. Optical Spectrum of Photons Subject to Synthetic Magnetic Field

We now explore numerically the full dynamics, beyond the perturbative limit. The optical local density of states (LDOS) is experimentally accessible by measuring the reflection when probing an optical defect mode via a tapered fiber, and it reveals the spectrum of the Hamiltonian. It thus provides a reasonable way to assess the validity of the effective Hamiltonian beyond the perturbative limit. Figure 2(a) shows the LDOS in the bulk calculated with the ideal effective Hofstadter model (1) for a spatially constant magnetic field, depicting the famous fractal Hofstadter butterfly structure [38]. For comparison, we plot the LDOS of the modulated-link scheme in Figs. 2(b) and 2(c). It is obtained by numerically calculating the Floquet Green's function of the full equations of motion (with time-periodic coefficients); see Supplement 1. The results indicate that the scheme works even for $J_{\rm eff} \sim 0.1\Omega > \kappa$, although perturbation theory clearly breaks down in this regime. We stress that the butterfly in Figs. 2(b) and 2(c) could even be observed experimentally at room temperature, since the spectrum is insensitive to thermal fluctuations. One would also observe sidebands; see Fig. 2(d). Similar results hold for the wavelength-conversion scheme (not shown here). Note that some states may not show up in the LDOS (or their contribution may be suppressed), depending on their wavefunction and the location. This is particularly true for the contribution of the edge states, since we chose a location in the middle of the sample. Nevertheless the features of the usual Hofstadter butterfly spectrum (which is the eigenvalue spectrum) manifest themselves in the experimentally accessible LDOS, as evidenced by Fig. 2(a).

B. Spatially Resolved Photon Transport

In addition to measuring the optical spectrum, it is also possible to look at photon transport in a spatially resolved manner, by injecting a probe laser locally and then imaging the photons leaving the sample. This provides another way to observe the effects of the artificial gauge field, which gives rise to distinct transport phenomena as depicted in Figs. 3(a) and 3(b). For small magnetic fields, $|\phi| \ll 2\pi$, the dynamics can be understood in the continuum limit when probing the bulk: one recovers the standard Landau level picture for electrons in a constant magnetic field [38,39], with effective mass $m^* = \hbar/2Ja^2$ and cyclotron frequency $\omega_{\rm cyc} = 2\phi J$, where a is the lattice constant. In Fig. 3(a) the $n = 1$ Landau level is selected via the probe's detuning Δ_p with respect to the drive. The circles indicate the semiclassical cyclotron orbits with radius $R = a\sqrt{(2n+1)/\phi}$. In this semiclassical picture, the momentum of a photon injected locally at a site in the bulk is equally distributed over all directions,

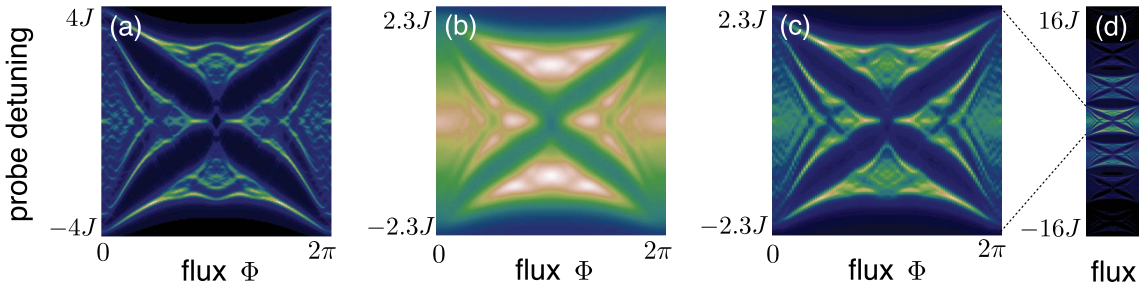

Fig. 2. Comparison between (a) experimentally accessible optical spectrum (LDOS) of the ideal effective Hofstadter model and (b)–(d) actual results from the proposed modulated-link scheme, for different optical decay rates and magnetic fluxes. The simulation results indicate that the scheme works even beyond the perturbative regime. The resulting Hofstadter butterfly could be observed by a local tapered fiber probe. Modulation of links produces higher sidebands (d). The phase configuration corresponds to a constant magnetic flux Φ per plaquette; see Fig. 1. [Parameters: grid (a) 10×10, (b)–(d) 12×12; (a)–(d) $J_{\rm eff} = 0.108\Omega_0$; (a),(c),(d) $\kappa = 0.01\Omega_0$, (b) $\kappa = 0.05\Omega_0$; (b)–(d) $J = 0.3\Omega_0$; (b)–(d) $g_0|\beta| = 0.3\Omega_0$; optical eigenfrequencies (relative to first mode) in a row (left to right) including interface modes: (b)–(d) $(0, 0.5, 1, 1.5, \ldots)\Omega_0$.]

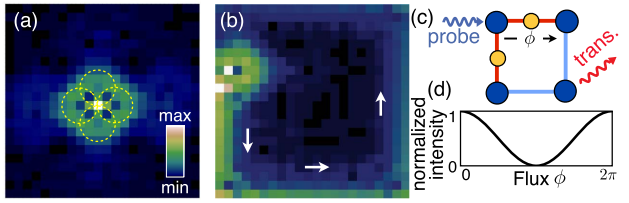

Fig. 3. Microscopic simulation of the wavelength-conversion scheme, Eq. (4), indicating its feasibility: spatial distribution of light intensity upon local injection of a probe laser (a) in the bulk and (b) at the edge, for a constant artificial magnetic field. Bulk transport (a) is governed by Landau levels and can be understood as a superposition of classical cyclotron orbits (yellow circles) for different momentum directions. (b) At the edges robust edge channels exist. (c) Optical Aharonov–Bohm effect in minimal symmetric setup. (d) The interference pattern (normalized probe laser transmission intensity) is shifted by the magnetic flux through the ring. [Parameters: (a),(b) 22×22 grid; (a),(b) $\delta = 0.3\Omega_0$, (d) $\delta = 0.1\Omega_0$; (a),(b) $g = 0.2\Omega_0$, (d) $g = 0.01\Omega_0$; (a),(b) $\kappa = 0.01\Omega_0$; $\Gamma = \kappa/10$; (a),(b) $\Phi = 2\pi/8$; (a),(b) $J = 0.13\Omega_0$, (d) $J = 0.001\Omega_0$, (a) $\Delta_p = 1.278\Omega_0$, (b) $\Delta_p = 1.260\Omega_0$, (d) $\Delta_p = 1.103\Omega_0$.]

since the position is well-defined. Thus, the observed response resembles a superposition of semiclassical circular Lorentz trajectories with different initial velocity directions. A probe injected closer to the edge excites chiral integer quantum Hall effect edge states; see Fig. 3(b).

The Aharonov–Bohm effect [40] is one of the most intriguing features of quantum mechanics. In an interferometer, electrons can acquire a phase difference determined by the magnetic flux enclosed by the interfering pathways, even though they never feel any force due to the magnetic field. Figure 3(c) depicts a setup that is based on the wavelength-conversion scheme and realizes an optical analog of the Aharonov–Bohm effect: a local probe is transmitted via two pathways, leading to an interference pattern in the transmission. The pattern is shifted according to the flux through the "ring" [see Fig. 3(d)], confirming the effect.

All the effects displayed in Fig. 3 have been simulated numerically for the wavelength-conversion scheme (see Supplement 1), but similar results hold for the modulated-link scheme.

4. GAUGE FIELDS IN SYNTHETIC DIMENSIONS

So far we have analyzed schemes to engineer hopping phases for photons. We now ask about situations in which the phonons are not only employed as auxiliary virtual excitations, but rather occur as real excitations, which can be interconverted with the photons. This means, in addition to the modes making up the lattices described above (in either of the two schemes), we now consider on-site vibrational modes $\hat{b}_j$ coupled optomechanically to the corresponding optical modes $\hat{a}_j$. Using the standard approach [1], we arrive at a linearized optomechanical interaction of the form $-g\hat{a}_j^\dagger \hat{b}_j + \text{h.c.}$ Moreover, to be general (and generate nontrivial features connected to the gauge field structure), we will assume that the neighboring phonon modes may also be coupled, as described by a tight-binding Hamiltonian of the form $-K\sum_{\langle ij\rangle} \hat{b}_j^\dagger \hat{b}_i + \text{h.c.}$

When discussing the effects of gauge fields in such a setting, the system is best understood within the concept of 'synthetic' dimensions [41–44]. The optomechanical interaction can be viewed in terms of an extension of the 1D or 2D lattice into such an additional synthetic dimension. In our case, this dimension only has two discrete locations, corresponding to photons versus phonons. In that picture, the optomechanical interaction, converting photons to phonons, corresponds to a simple hopping between sites along the additional direction. Figure 4(a) sketches this for an optomechanical ring: photons and phonons represent two layers separated along the synthetic dimension. Applying any of our two previously discussed schemes, a photon hopping from site i to j will acquire a phase $\phi_{ij} = \int_{\mathbf{r}_i}^{\mathbf{r}_j} d\mathbf{r}\mathbf{A}$. The gauge field $\mathbf{A}$ must now be viewed as a vector field in this new three-dimensional (3D) space, where one of the dimensions is synthetic. A finite hopping phase ϕ at one of the optical links creates a magnetic flux through the optical plaquette as desired; see Fig. 4(a). However, and this is the important point, since the magnetic field $\mathbf{B}$ is divergence-free, the field must penetrate at least one additional plaquette, causing the opposite magnetic flux in the synthetic dimension (assuming $g \in \mathbb{R}$). In general, realizing that there is this kind of behavior is crucial to avoid puzzles about seeming violations of gauge symmetry in situations with photon magnetic fields in optomechanical arrays. It is necessary to keep track of the full vector potential in the space that includes the synthetic dimension.

We now take a step back, getting rid of the previously discussed engineered schemes that required two lasers and some arrangement of 'link' modes. Rather we will consider simple optomechanical arrays, i.e., lattices of optical and vibrational modes, with photon and phonon tunnel coupling between modes and with the optomechanical interaction. We ask: What is the effect of an arbitrary, spatially varying optical phase field in the driving laser that sets the strength of the optomechanical coupling? It turns out that the resulting spatially varying phase of the optomechanical coupling, $g_j = |g_j|e^{i\varphi_j}$, can be chosen to create arbitrary magnetic fields perpendicular to the synthetic dimension. A particularly simple example is a simple linear chain of optomechanical cells. Shining a tilted laser (i.e., with a phase gradient, $\varphi_j = j \cdot \delta\varphi$) onto such a 1D optomechanical array creates a constant magnetic flux through the plaquettes of the "optomechanical synthetic ladder" that can be drawn to understand the situation; cf. Fig. 4(b). The quantum mechanics

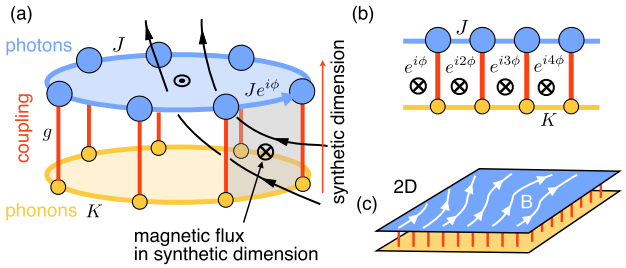

Fig. 4. Optomechanical gauge fields within the concept of synthetic dimensions. (a) The optomechanical coupling, g, can be viewed as connecting sites along a synthetic dimension (photons versus phonons). A phase for the photon hopping, engineered using the schemes from above, creates a flux in the optical plaquette (blue, top) and in the adjacent synthetic plaquette (gray). Hence, the magnetic field (black lines) in the full space is divergence-free. (b) Engineering exclusively the phases of g allows us to create magnetic fields/fluxes, but only perpendicular to the synthetic dimension. Shining a single tilted laser on a 1D chain yields a synthetic optomechanical ladder system with constant synthetic magnetic flux. (c) 2D array, with the field inside the (physical) plane generated by an arbitrary laser phase pattern.

of excitations tunneling between the two 'rails' of the ladder (corresponding to photon–phonon conversion) are directly analogous to experiments on electron tunneling between parallel wires in a magnetic field [45]. The magnetic field shifts the momenta of the tunneling particles, giving rise to resonance phenomena when the shifted dispersion curves $\omega(k)$ of the excitations match. Via phase front engineering one could create arbitrary synthetic magnetic fields also in 2D grids; see Fig. 4(c). We note, though, that this method is constrained since it cannot directly create magnetic fluxes through optical or mechanical plaquettes, and in general only the schemes discussed above provide full flexibility. On the other hand, if either the photon or the phonon modes are occupied only virtually, then effective fluxes can still be generated for the remaining real excitations, even with a single laser, and this works best for phonons (see [46,47]).

5. POSSIBLE EXPERIMENTAL REALIZATIONS

We now discuss the most salient aspects of the experimental realization. Both the 'butterfly' optical spectrum and spatially resolved transport can be probed using homodyne techniques, which are insensitive to noise. Real-space optical imaging is feasible, as the defects are a few micrometers apart. The optical phase pattern can be engineered using spatial light modulators. No time-dependent changes of the pattern are needed here, since the time dependence is generated via the beat-note between the two laser beams.

For the modulated-link scheme, the mechanical oscillation amplitude β used for the modulation should overwhelm any thermal fluctuations. In the example of Fig. 2, we assumed $g_0\beta = 0.3\Omega_0$. At recently achieved parameters [7] $g_0/2\pi = 220$ kHz and $\Omega_0/2\pi = 9$ GHz, this would imply $\beta \sim 10^4$, i.e., a phonon number of 10^8 reached by driving, certainly larger than the thermal population. If we drive the mechanical vibration using a radiation pressure force oscillating at resonance (assuming the quoted g_0 also for the optical mode used in that driving), then we have $\beta = 2g_0 n_c/\Gamma$, where n_c is the circulating photon number and Γ is the mechanical damping rate. Given a mechanical quality factor of $\Omega_0/\Gamma = 2 \cdot 10^5$, this requires $n_c \sim 10^3$ photons for Fig. 2, a realistic number. We note that thermal fluctuations of the mechanical amplitude give rise to a fractional deviation of $\sqrt{\bar{n}_{\rm th}}/\beta$ in $J_{\rm eff}$, with a slow drift on the time scale Γ^{-1}. At typical temperatures used in experiments, we have $\bar{n}_{\rm th} \sim 100$ – 1000, and so the fractional change is on the order of a percent, which will not noticeably impact transport.

In the alternative wavelength-conversion scheme, one should strive for a large photon-enhanced optomechanical coupling rate $g = g_0\alpha$. A general estimate implies that we always need the photon number to be larger than $(\kappa/g_0)^2$ in order to see the butterfly spectrum and the transport effects. This condition (compatible with Fig. 3) would require a circulating photon number of around $3 \cdot 10^5$ for the parameters demonstrated in a recent successful wavelength-conversion setup based on optomechanical crystals [36]. It is also important to estimate the unwanted influx of thermal excitations from the phonon subsystem into the photon subsystem, at least if the setup is to be applied in the quantum regime, for observing the transport of *single* photons in the presence of a magnetic field. In the wavelength-conversion scheme, there is a detuning $\delta \gg \kappa$ between the red sideband of the laser and the phonon mode, such that photon–phonon conversion is suppressed. Nevertheless, it still happens at a rate $\gamma\bar{n}$, where $\gamma = g^2/\delta$ is the "cooling rate" (for the detuned case applicable here) and $\bar{n}$ is the number of phonons in the mode. Fortunately, this phonon number is also reduced by the very same off-resonant cooling process. Balancing the inflow and outflow of excitations, we find that there will be a remaining unwanted photon occupation of $\bar{n}^{\rm th}_{\rm phot} = \bar{n}_{\rm th}\Gamma/\kappa$ due to the conversion of thermal phonons into photons, where $\bar{n}_{\rm th}$ is the bulk thermal phonon occupation. The factor Γ/κ suppresses this number strongly, and it should be possible to reach the regime $\bar{n}^{\rm th}_{\rm phot} \ll 1$ in low-temperature setups.

Reducing fabrication-induced disorder will be crucial for any future applications of photonic crystals, including the one envisaged here (as well as other photonic magnetic field schemes). In first experimental attempts, the optical and mechanical disorder is on the percent level, which makes especially the fluctuations of the optical resonance frequencies significant. Nevertheless, strong reductions of the disorder will be possible by post-fabrication methods [48–50], such as local laser-induced oxidation. These are expected to reduce the fluctuations down to the level of 10^{-5} relative optical frequency fluctuations. This is enough to suppress the optical disorder to some fraction of the photon hopping rate $J_{\rm eff} \sim \Omega$, which will enable near-ideal photon transport (e.g., Anderson localization lengths would be at least hundreds of sites, larger than the typical arrays). Disorder in the mechanical frequencies can be reduced by similar techniques, but is much less problematic, due to the difference in absolute frequency scales between optics and mechanics.

6. OUTLOOK

Optomechanical crystals represent an interesting system for the realization of artificial photonic magnetic fields. The fact that the magnetic field is not generated by the geometry of device fabrication but rather controlled all-optically offers the significant advantage of *in situ* tunability. At the same time, the robustness of the resulting edge states against backscattering by disorder is better than in topological-insulator inspired photonic schemes, since the latter are still susceptible to certain kinds of disorder.

The rich nonlinear (quantum) dynamics [10] of optomechanical arrays could be explored in the presence of such an artificial magnetic field. In general, the very flexible optical control could be used to create and explore novel features, e.g., varying the optomechanical coupling strength spatially and/or temporally, both adiabatically and with sudden quenches. Moreover, a second strong control laser could be used to create a spatially and temporarily varying optical on-site potential landscape, such that the combined effect of that potential and the magnetic field on the photon transport can be explored.

Funding. Defense Advanced Research Projects Agency (DARPA) (ORCHID); European Commission (EC) (Marie-Curie ITN cQOM); European Research Council (ERC) (Starting Grant OPTOMECH).

Acknowledgment. We thank an anonymous referee for pointing out to us the work of Kolovsky.

See Supplement 1 for supporting content.

REFERENCES

1. M. Aspelmeyer, T. J. Kippenberg, and F. Marquardt, "Cavity optomechanics," Rev. Mod. Phys. **86**, 1391 (2014).
2. A. H. Safavi-Naeini and O. Painter, "Design of optomechanical cavities and waveguides on a simultaneous bandgap phononic-photonic crystal slab," Opt. Express **18**, 14926–14943 (2010).
3. M. Eichenfield, J. Chan, R. M. Camacho, K. J. Vahala, and O. Painter, "Optomechanical crystals," Nature **462**, 78–82 (2009).
4. A. H. Safavi-Naeini, T. P. M. Alegre, M. Winger, and O. Painter, "Optomechanics in an ultrahigh-q two-dimensional photonic crystal cavity," Appl. Phys. Lett. **97**, 181106 (2010).
5. E. Gavartin, R. Braive, I. Sagnes, O. Arcizet, A. Beveratos, T. J. Kippenberg, and I. Robert-Philip, "Optomechanical coupling in a two-dimensional photonic crystal defect cavity," Phys. Rev. Lett. **106**, 203902 (2011).
6. J. Chan, T. P. M. Alegre, A. H. Safavi-Naeini, J. T. Hill, A. Krause, S. Groblacher, M. Aspelmeyer, and O. Painter, "Laser cooling of a nanomechanical oscillator into its quantum ground state," Nature **478**, 89–92 (2011).
7. A. H. Safavi-Naeini, J. T. Hill, S. Meenehan, J. Chan, S. Gröblacher, and O. Painter, "Two-dimensional phononic-photonic band gap optomechanical crystal cavity," Phys. Rev. Lett. **112**, 153603 (2014).
8. G. Heinrich, M. Ludwig, J. Qian, B. Kubala, and F. Marquardt, "Collective dynamics in optomechanical arrays," Phys. Rev. Lett. **107**, 043603 (2011).
9. C. A. Holmes, C. P. Meaney, and G. J. Milburn, "Synchronization of many nanomechanical resonators coupled via a common cavity field," Phys. Rev. E **85**, 066203 (2012).
10. M. Ludwig and F. Marquardt, "Quantum many-body dynamics in optomechanical arrays," Phys. Rev. Lett. **111**, 073603 (2013).
11. M. Bhattacharya and P. Meystre, "Multiple membrane cavity optomechanics," Phys. Rev. A **78**, 041801 (2008).
12. A. Xuereb, C. Genes, and A. Dantan, "Strong coupling and long-range collective interactions in optomechanical arrays," Phys. Rev. Lett. **109**, 223601 (2012).
13. A. Tomadin, S. Diehl, M. D. Lukin, P. Rabl, and P. Zoller, "Reservoir engineering and dynamical phase transitions in optomechanical arrays," Phys. Rev. A **86**, 033821 (2012).
14. M. Schmidt, M. Ludwig, and F. Marquardt, "Optomechanical circuits for nanomechanical continuous variable quantum state processing," New J. Phys. **14**, 125005 (2012).
15. U. Akram, W. Munro, K. Nemoto, and G. J. Milburn, "Photon-phonon entanglement in coupled optomechanical arrays," Phys. Rev. A **86**, 042306 (2012).
16. D. E. Chang, A. H. Safavi-Naeini, M. Hafezi, and O. Painter, "Slowing and stopping light using an optomechanical crystal array," New J. Phys. **13**, 023003 (2011).
17. W. Chen and A. A. Clerk, "Photon propagation in a one-dimensional optomechanical lattice," Phys. Rev. A **89**, 033854 (2014).
18. M. Schmidt, V. Peano, and F. Marquardt, "Optomechanical Dirac physics," New J. Phys. **17**, 023025 (2015).
19. J. Koch, A. A. Houck, K. L. Hur, and S. M. Girvin, "Time-reversal-symmetry breaking in circuit-QED-based photon lattices," Phys. Rev. A **82**, 043811 (2010).
20. M. Hafezi, E. A. Demler, M. D. Lukin, and J. M. Taylor, "Robust optical delay lines with topological protection," Nat. Phys. **7**, 907–912 (2011).
21. R. O. Umucalılar and I. Carusotto, "Artificial gauge field for photons in coupled cavity arrays," Phys. Rev. A **84**, 043804 (2011).
22. K. Fang, Z. Yu, and S. Fan, "Realizing effective magnetic field for photons by controlling the phase of dynamic modulation," Nat. Photonics **6**, 782–787 (2012).
23. M. Hafezi and P. Rabl, "Optomechanically induced non-reciprocity in microring resonators," Opt. Express **20**, 7672–7684 (2012).
24. M. Hafezi, S. Mittal, J. Fan, A. Migdall, and J. M. Taylor, "Imaging topological edge states in silicon photonics," Nat. Photonics **7**, 1001–1005 (2013).
25. S. Mittal, J. Fan, S. Faez, A. Migdall, J. M. Taylor, and M. Hafezi, "Topologically robust transport of photons in a synthetic gauge field," Phys. Rev. Lett. **113**, 087403 (2014).
26. M. C. Rechtsman, J. M. Zeuner, Y. Plotnik, Y. Lumer, D. Podolsky, F. Dreisow, S. Nolte, M. Segev, and A. Szameit, "Photonic Floquet topological insulators," Nature **496**, 196–200 (2013).
27. Y. J. Lin, R. L. Compton, K. Jimenez-Garcia, J. V. Porto, and I. B. Spielman, "Synthetic magnetic fields for ultracold neutral atoms," Nature **462**, 628–632 (2009).
28. A. Bermudez, T. Schaetz, and D. Porras, "Synthetic gauge fields for vibrational excitations of trapped ions," Phys. Rev. Lett. **107**, 150501 (2011).
29. M. Aidelsburger, M. Atala, M. Lohse, J. T. Barreiro, B. Paredes, and I. Bloch, "Realization of the Hofstadter Hamiltonian with ultracold atoms in optical lattices," Phys. Rev. Lett. **111**, 185301 (2013).
30. H. Miyake, G. A. Siviloglou, C. J. Kennedy, W. C. Burton, and W. Ketterle, "Realizing the Harper Hamiltonian with laser-assisted tunneling in optical lattices," Phys. Rev. Lett. **111**, 185302 (2013).
31. L. D. Tzuang, K. Fang, P. Nussenzveig, S. Fan, and M. Lipson, "Non-reciprocal phase shift induced by an effective magnetic flux for light," Nat. Photonics **8**, 701–705 (2014).
32. G. Heinrich, J. G. E. Harris, and F. Marquardt, "Photon shuttle: Landau-Zener-Stückelberg dynamics in an optomechanical system," Phys. Rev. A **81**, 011801 (2010).
33. A. R. Kolovsky, "Creating artificial magnetic fields for cold atoms by photon-assisted tunneling," Europhys. Lett. **93**, 20003 (2011).
34. C. E. Creffield and F. Sols, "Comment on 'Creating artificial magnetic fields for cold atoms by photon-assisted tunneling' by Kolovsky A. R.," Europhys. Lett. **101**, 40001 (2013).
35. M. Aidelsburger, M. Atala, S. Nascimbène, S. Trotzky, Y.-A. Chen, and I. Bloch, "Experimental realization of strong effective magnetic fields in optical superlattice potentials," Appl. Phys. B **113**, 1–11 (2013).
36. J. T. Hill, A. H. Safavi-Naeini, J. Chan, and O. Painter, "Coherent optical wavelength conversion via cavity-optomechanics," Nat. Commun. **3**, 1196 (2012).
37. C. Dong, V. Fiore, M. C. Kuzyk, and H. Wang, "Optomechanical dark mode," Science **338**, 1609–1613 (2012).
38. D. R. Hofstadter, "Energy levels and wave functions of Bloch electrons in rational and irrational magnetic fields," Phys. Rev. B **14**, 2239–2249 (1976).
39. L. D. Landau and E. M. Lifshitz, *Statistical Physics, Part 2* (Butterworth-Heinemann, 1980).
40. Y. Aharonov and D. Bohm, "Significance of electromagnetic potentials in the quantum theory," Phys. Rev. **115**, 485–491 (1959).
41. O. Boada, A. Celi, J. I. Latorre, and M. Lewenstein, "Quantum simulation of an extra dimension," Phys. Rev. Lett. **108**, 133001 (2012).
42. A. Celi, P. Massignan, J. Ruseckas, N. Goldman, I. B. Spielman, G. Juzeliunas, and M. Lewenstein, "Synthetic gauge fields in synthetic dimensions," Phys. Rev. Lett. **112**, 043001 (2014).
43. M. Mancini, G. Pagano, G. Cappellini, L. Livi, M. Rider, J. Catani, C. Sias, P. Zoller, M. Inguscio, M. Dalmonte, and L. Fallani, "Observation of chiral edge states with neutral fermions in synthetic Hall ribbons," arXiv:1502.02495 (2015).
44. B. K. Stuhl, H.-I. Lu, L. M. Aycock, D. Genkina, and I. B. Spielman, "Visualizing edge states with an atomic Bose gas in the quantum Hall regime," arXiv:1502.02496 (2015).
45. H. Steinberg, G. Barak, A. Yacoby, L. N. Pfeiffer, K. W. West, B. I. Halperin, and K. Le Hur, "Charge fractionalization in quantum wires," Nat. Phys. **4**, 116–119 (2008).
46. S. J. M. Habraken, K. Stannigel, M. D. Lukin, P. Zoller, and P. Rabl, "Continuous mode cooling and phonon routers for phononic quantum networks," New J. Phys. **14**, 115004 (2012).
47. V. Peano, C. Brendel, M. Schmidt, and F. Marquardt, "Topological phases of sound and light," arXiv:1409.5375 (2014).
48. J. Zheng, C. J. Chen, J. F. McMillan, M. Yu, G.-Q. Lo, D.-L. Kwong, and C. W. Wong, "Selective tuning of silicon photonic crystal cavities via laser-assisted local oxidation," in *Conference on Lasers and Electro-Optics (CLEO)*, May 1–6, 2011, pp. 1–2.
49. H. S. Lee, S. Kiravittaya, S. Kumar, J. D. Plumhof, L. Balet, L. H. Li, M. Francardi, A. Gerardino, A. Fiore, A. Rastelli, and O. G. Schmidt, "Local tuning of photonic crystal nanocavity modes by laser-assisted oxidation," Appl. Phys. Lett. **95**, 191109 (2009).
50. K. Hennessy, C. Högerle, E. Hu, A. Badolato, and A. Imamoglu, "Tuning photonic nanocavities by atomic force microscope nano-oxidation," Appl. Phys. Lett. **89**, 041118 (2006).